Helicenes

Deutsche Ausgabe: DOI: 10.1002/ange.201607878
Internationale Ausgabe: DOI: 10.1002/anie.201607878

Electron Delocalization in Perylene Diimide Helicenes

Nathaniel J. Schuster, Daniel W. Paley, Steffen Jockusch, Fay Ng, Michael L. Steigerwald, and Colin Nuckolls**

Abstract: *We report two new helicenes derived from the double fusion of an acene with two perylene diimide (PDI) subunits. These PDI-helicene homologs exhibit very different structural and electronic properties, despite differing by only a single ring in the link between the PDI units. The shorter inter-PDI link brings the two PDI subunits closer together, and this results in the collision of their respective π-electron clouds. This collision facilitates intramolecular through-space electronic delocalization when the PDI-helicene is reduced.*

Here we describe new perylene-diimide-based molecules that demonstrate how narrowing the distance between redox-active subunits can reinforce the delocalization of electrons added to a fully conjugated helical framework. Perylene-3,4,9,10-tetracarboxylic diimide (PDI) provides a wellspring of intensely absorbing, robust dye materials with substantial electron affinities.[1] Readily prepared and easily derivatized, these materials excel as n-type semiconductors[2–4] in organic field effect transistors[5,6] and organic photovoltaics (OPVs).[7,8] Some of the most efficient non-fullerene-based OPVs incorporate oligomeric PDI-nanoribbons.[9–11] In these nanoribbons, a succession of steric interactions contort the π-surface to form a twistacene (Figure 1 a)—a polyaromatic helix in which the stereogenic axis transects the core of the molecule.[12] By coiling PDI-based nanoribbons about an alternative axis (Figure 1 b), new helical scaffolds—PDI-helicenes—can be realized.

A helicene consists of angularly fused aromatic subunits arranged consecutively in a helix. Its π-surface coils around a nonintersecting stereogenic axis to give a strained cylindrical core. This strain often encumbers the synthesis of helicenes,[13,14] but they remain compelling targets due to their wealth of fascinating chiral and chiroptical properties.[15] Additionally, π-to-π interactions between redox-active quinones within helicene radical anions have been shown to enhance electronic delocalization[16,17] and to promote the assembly of chiral supramolecular aggregates with pronounced nonlinear optical properties.[18,19] More recently, installing vinyl ruthenium and alkynyl iron complexes on the termini of [6]helicene has been shown to amplify the chiroptical properties of the helicene core, as well as to enable redox-triggered chiroptical switching.[20–22] Thus, by integrating redox-active PDI into helicenes, we intended to combine the desirable properties of both types of molecular structures into a single nanoribbon.

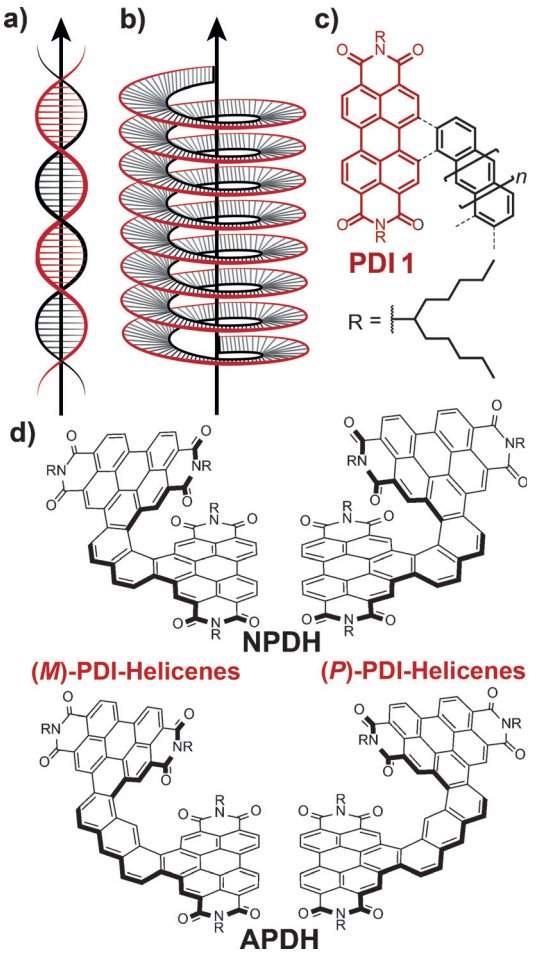

Figure 1. The helical contortion of PDI-nanoribbons to make a) twistacenes or b) helicenes. c) Acene fusion with the bay of the PDI yields PDI-helicenes ($n=0$ and 1). d) Fusion with two PDI moieties forms (*M*)- and (*P*)-**NPDH** and (*M*)- and (*P*)-**APDH**.

This manuscript details the synthesis and characterization of two new helicenes that result from the double fusion along one of the zigzag edges of an acene with the bay of two PDI monomers (Figure 1 c, $n=0$ and 1). Fusion with naphthalene or anthracene forms naphthyl- or anthracenyl-linked PDI-dimer helicene (**NPDH** and **APDH**). We separated the left-(*M*) and right-handed (*P*) helicenes of both compounds (Figure 1 d) and discovered that **NPDH** resists racemization at very high temperatures (>250 °C). The enantiomers of **APDH** interconvert at room temperature. Intermolecular π-to-π stacking mediates the self-assembly of single-handed

[*] N. J. Schuster, Dr. D. W. Paley, Dr. S. Jockusch, Dr. F. Ng, Dr. M. L. Steigerwald, Prof. C. Nuckolls
Chemistry Department, Columbia University
New York, NY 10027 (USA)
E-mail: mls2064@columbia.edu
cn37@columbia.edu

Supporting information for this article can be found under: http://dx.doi.org/10.1002/anie.201607878.

supramolecular helixes of **APDH** in the solid state. The large gap separating the PDI subunits of **APDH** minimizes intramolecular π-to-π contact. Conversely, the [6]helicene core of **NPDH** positions its PDI subunits within 3.2 Å of one another. This proximity facilitates the intramolecular collision of their π-electron clouds, which enhances the delocalization of electrons added to **NPDH**.

Scheme 1 illustrates the simple synthetic route to prepare **NPDH** and **APDH** in near-quantitative yields. Our strategy stemmed largely from two previous findings: 1) bromination can occur exclusively at the bay position of *N*,*N*′-dialkylated

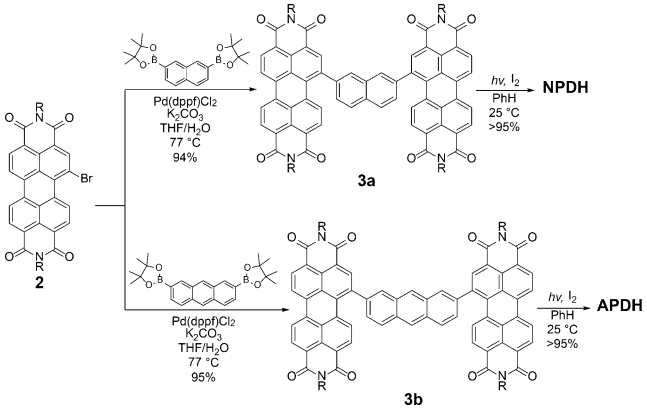

Scheme 1. Two-step synthesis of PDI-helicenes **NPDH** and **APDH** from brominated PDI **2** [R = CH(C$_5$H$_{11}$)$_2$].

PDI;[23] and 2) acenes fuse preferentially at their *peri*-positions during intramolecular oxidative photocyclizations,[24] particularly with PDI and its precursors.[25–27] Accordingly, we prepared **NPDH** and **APDH** in two steps from brominated PDI **2**. First, the Suzuki–Miyaura cross-coupling[28] of **2** with either 2,7-diborylated naphthalene or 2,7-diborylated anthracene afforded the acene-bridged PDI dimers **3a** or **3b**, respectively. Subsequent oxidative ultraviolet photocyclizations of these intermediates provided **NPDH** and **APDH** as racemates in quantitative yields. As such, trituration and filtration were sufficient to obtain analytically pure **NPDH** and **APDH** as orange and red solids, respectively. There was no indication, in either case, of cyclization at the alternative *ortho*-position of the acenes. Due to their contorted conformations and four branched alkyl tails, both PDI-helicenes dissolved readily in a variety of organic solvents, including dichloromethane (DCM), benzene (PhH), and tetrahydrofuran (THF). They were practically insoluble in methanol, ethanol, and hexanes.

We readily separated the (*M*)- and (*P*)-PDI-helicenes of **NPDH** and **APDH** using chiral HPLC (see Figure S1 in the Supporting Information) and examined their resistance to thermally induced racemization. Analysis of the previously resolved samples of **APDH** by chiral HPLC revealed that its enantiomers interconvert at room temperature in solution. Conversely, the steric congestion intrinsic to the [6]helicene core of **NPDH** significantly impedes inversion. Remarkably, a single enantiomer of **NPDH** heated at 250 °C in diphenyl ether for one hour showed no isomerization. For comparison, enantiopure [6]helicene racemizes completely in solution in about 13 minutes at 220 °C,[29] and a recently reported π-extended double [6]helicene isomerizes in solution at 230 °C.[30] Its ease of synthesis and enantiostability at high temperatures make **NPDH** an excellent candidate for various applications in chiral nanoscience, a conclusion reinforced by the wealth and intensity of the circular dichroism (CD) transitions of its enantiomers (Figure 2). The particularly pronounced Cotton effect at 523 nm underscores the synergistic combination of the inherent chirality of [6]helicene with the strong absorptivity of the PDI chromophores.

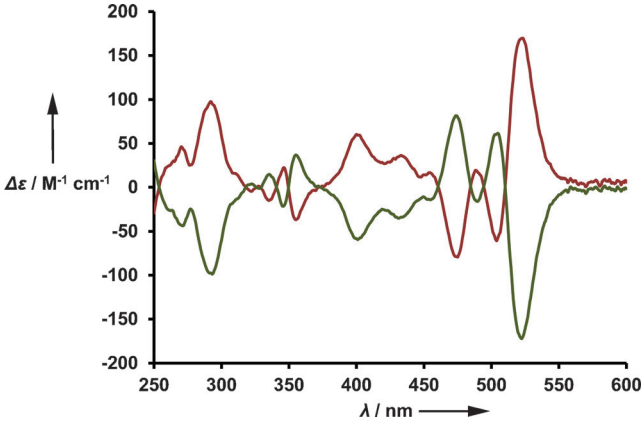

Figure 2. CD spectra of (*M*)- and (*P*)-**NPDH** in THF (10 μM, 1 cm pathlength).

We further investigated the molecular structures of **NPDH** and **APDH** using density functional theory (DFT) and single-crystal X-ray diffraction (SCXRD). Solutions of racemic **APDH** readily yielded crystals of sufficient quality for SCXRD. The solid-state structure (Figure 3a) closely resembles the DFT-optimized, gas-phase model of **APDH** (Figure S2). DFT shows the planes within the two perylene cores of each PDI bisect at 45°, whereas in the solid state the same angle measures 49°. Looking down the stereogenic axis of **APDH** reveals that four pairs of π-bonded atoms eclipse one another (Figure S3a). The splaying of the π-surface in the solid state separates the nearest of these eclipsing pairs by 5.7 Å (5.8 Å in the gas-phase structure). This distance exceeds the range of substantive π-to-π interaction. The crystal structure of **APDH** reveals extensive intermolecular π-to-π interactions between the helicenes, with successive PDI pairs slip-stacking cofacially within 3.4 Å of each other (Figure 3b). These interactions guide the formation of supramolecular helixes that complete one revolution every third helicene (Figures S3b and S3c). The enantiomers of **APDH** impart their chirality to the helixes: (*P*)-helicenes form (*P*)-helixes while (*M*)-helicenes form (*M*)-helixes within a racemic crystal.

We have been unable to grow crystals of **NPDH** of sufficient quality for SCXRD. Nevertheless, the rigidity of **NPDH** suggests the DFT model (Figure 3c) adequately represents its molecular structure. Similar to **APDH**, the PDI planes in **NPDH** intersect at a 48° angle, although this distortion does not open a significant gap between the PDI

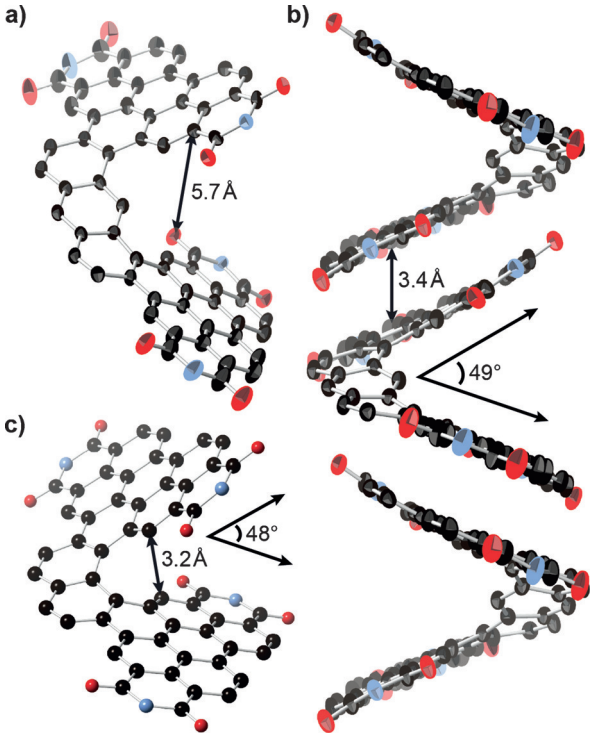

Figure 3. a) Structure of (*M*)-**APDH** from SCXRD. b) Left-handed supramolecular helix assembled in the solid state. Free solvent, the $CH(C_5H_{11})_2$ tails, and hydrogen atoms have been removed to provide a better view of the π-surface. Thermal ellipsoids are set at 20% probability. c) DFT-optimized model of (*M*)-**NPDH** (B3LYP/6-31G**). Its methyl groups, which substitute for the $CH(C_5H_{11})_2$ tails to simplify the calculation, and hydrogen atoms have been removed in the image.

subunits. Looking down the stereogenic axis of **NPDH** shows that ten pairs of π-bonded atoms eclipse one another (Figure S4). This model predicts the distance between the nearest of these eclipsing pairs in **NPDH** to be 3.2 Å, well within twice the van der Waals radius of the carbon atom (3.4 Å). As such, we expected intramolecular π-to-π collisions to assist in delocalizing electrons subsequently added to **NPDH**.

UV/Vis absorbance spectroscopy provided evidence of enhanced intramolecular through-space excitonic coupling between the PDI subunits of **NPDH** relative to those of **APDH** (Figure 4). Both dimers retain the characteristic vibronic progression of the monomer PDI **1** (0-0 transition: $\lambda_{max} = 525$ nm); however, their corresponding progressions are shifted hypsochromically (0-0 transitions: $\lambda_{max} = 516$ nm and 497 nm for **NPDH** and **APDH**, respectively). Intensification of the 0-1 transition relative to the 0-0 transition in this progression indicates the enhancement of through-space excitonic coupling between the PDI chromophores.[31] Consistent with the relative distances separating their PDI subunits, **NPDH** exhibits a larger 0-1:0-0 transition ratio than **APDH**. PDI dimers with similarly stacked chromophores also exhibit intensification of the 0:1 transition.[32–36] However, conjugation between the chromophores in these previous dimers is inhibited by the use of linkers orthogonal to the π-surface of the PDI subunits.

The UV/Vis spectra of the PDI-helicenes differ significantly in one respect: the lowest-energy absorptions of

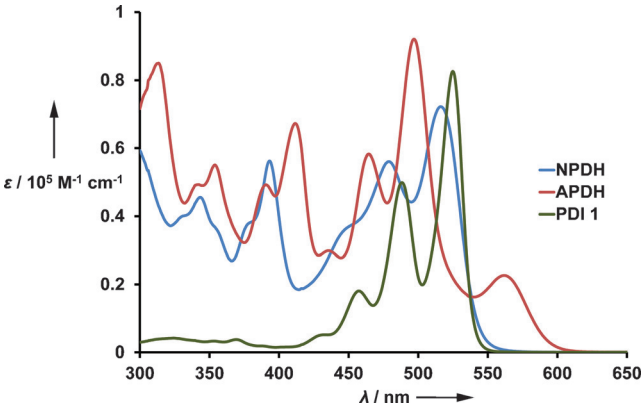

Figure 4. UV/Vis absorbance spectra of PDI **1**, **NPDH**, and **APDH** in DCM (10 μM, 1 cm pathlength).

NPDH resemble the vibronic progression of PDI **1**, whereas the lowest-energy absorption of **APDH** ($\lambda_{max} = 561$ nm) manifests as a broad band. DFT calculations indicate that the HOMO of **APDH** (Figure S5) localizes on the electron-rich anthracenyl link. The LUMOs of both PDI-helicenes (Figures S5 and S6) distribute across the electron-poor PDI subunits. Thus, the broad band in **APDH** corresponds to anthracene-to-PDI intramolecular charge transfer (ICT). Excitation of **APDH** at 561 nm generates emission peaks that shift bathochromically with increasing solvent polarity, ranging from 575 nm in toluene to 623 nm in *N*,*N*-dimethylacetamide. This positive solvatochromism supports our assignment of the least energetic absorption of **APDH** as ICT.[37] For **NPDH**, the HOMO delocalizes across the naphthyl link and PDI subunits, but the HOMO-2 lies primarily on the naphthyl link (Figure S6). Thus, acene-to-PDI ICT bands in **NPDH** originate from the HOMO-2, although they are obscured by intense electronic transitions in this region of the spectrum.

Electrochemical reductions of **NPDH** and **APDH** provided insight into the extent to which their anions delocalize electrons. The cyclic voltammetry (CV) reduction waves of both helicenes (Figure 5a) are reversible. The first reduction of **NPDH** and **APDH** is cathodically shifted by 100 mV relative to PDI **1**, which arises from the LUMO-raising effect of the electron-donating acene links.[38] Despite differing by only a single ring, **NPDH** and **APDH** generate very different voltammograms. Whereas **APDH** displays two clear reduction events, **NPDH** exhibits four reduction events grouped in two pairs. Spectroelectrochemical measurements (Figures S7 and S8) and, in particular, the four sets of isosbestic points shared by sequential pairs of oxidation states (e.g., **NPDH**/**NPDH**$^{\bullet-}$, **NPDH**$^{\bullet-}$/**NPDH**$^{2-}$, etc.) confirm that each event in the voltammogram of **NPDH** corresponds to a one-electron addition, while each event in **APDH** corresponds to the addition of two electrons. Therefore, both dimers can accept four electrons, although the second and fourth reductions of **NPDH** must overcome greater Coulombic repulsion than the corresponding reductions of **APDH**. This repulsion suggests **NPDH** possesses an enhanced ability to delocalize the first and third added electrons, which cathodically shifts the second and fourth reductions.

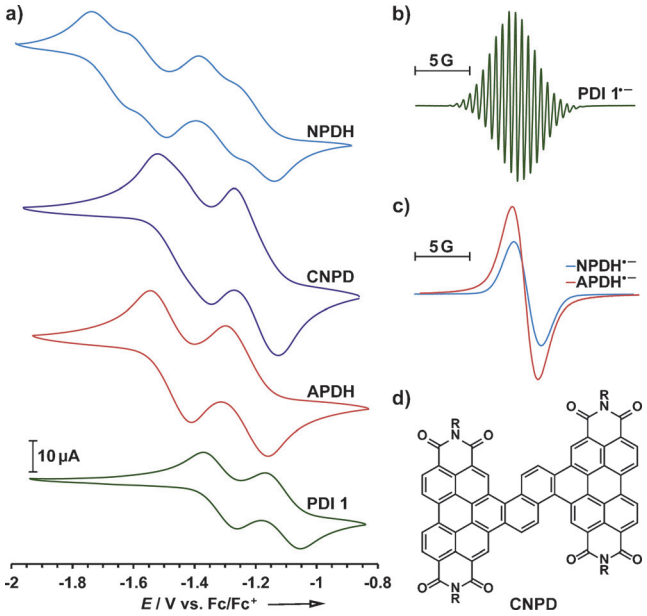

Figure 5. a) Cyclic voltammograms of monomeric PDI **1**, **APDH**, **CNPD**, and **NPDH** in Ar-sparged DCM (1 mM) with 0.1 M $[Bu_4N][PF_6]$ as the supporting electrolyte. Continuous-wave EPR spectra at 240 K of monoreduced b) PDI **1** and c) **APDH** and **NPDH** in DCM. d) Structure of **CNPD** $[R = CH(C_5H_{11})_2]$.

The electrochemical differences between **NPDH** and **APDH** originate from the intramolecular orientation of their PDI subunits. Through-bond electronic coupling between the four redox-active imide groups can occur by two routes in these dimers: 1) across their perylene cores, an effective delocalizing conduit as demonstrated previously for monomeric PDI;[39] and 2) through their contorted acene links. Dimers with noninteracting PDI subunits would generate voltammograms comparable to that of PDI **1**—two peaks separated by a potential of 200 mV. Instead, the reduction events in **APDH** differ by a potential of 250 mV, whereas their analogs in **NPDH** (i.e., 1^- to 3^- and 2^- to 4^-) differ by 350 mV. Accordingly, the PDI subunits couple electronically to one another in both dimers, but more strongly in **NPDH**. Continuous-wave EPR spectroscopy reaffirms that the PDI subunits in these helicenes share an added electron: whereas the spectrum of $\mathbf{1}^{\bullet-}$ shows extensive hyperfine splitting (Figure 5b), the spectra of $\mathbf{NPDH}^{\bullet-}$ and $\mathbf{APDH}^{\bullet-}$ do not (Figure 5c). This absence of hyperfine splitting for the PDI-helicene monoanions indicates the distribution of the radical electron across a π-surface larger than that of PDI **1**. Electron sharing over multiple PDI subunits within nanowires,[40,41] DNA hairpins,[42] and a molecular triangle[43] results in a similar loss of spectroscopic hyperfine structure.

The large gap separating the PDI subunits in **APDH** mitigates intramolecular π-to-π contact. Conversely, collisions between the π-clouds of the PDI subunits of **NPDH** reinforce through-bond coupling to enhance electronic delocalization in the anions of this helicene. To better examine the role of these intramolecular π-cloud collisions in facilitating electronic delocalization in reduced **NPDH**, we synthesized a contorted naphthyl-linked PDI dimer (**CNPD**, Figure 5d). This regioisomer of **NPDH** also has a twisted naphthyl link but orients its PDI subunits away from one another; thus, CV can assess through-bond electronic coupling between the PDI subunits in the absence of intramolecular π-to-π contact. The voltammogram of **CNPD** (Figure 5a) exhibits two broad reduction events that differ at most by 250 mV, suggestive of a diminished capacity to delocalize electrons relative to reduced **NPDH**. Therefore, intramolecular π-to-π collisions between the PDI subunits of **NPDH** reinforce the through-bond coupling mediated by the contorted naphthyl link to delocalize electrons in the reduced PDI-helicene.

In summary, we have developed an expeditious, high yielding synthesis of two acene-linked PDI-dimer helicenes, **NPDH** and **APDH**. Simply by tailoring the length of the acene link, we have instilled markedly different properties in these PDI-helicene homologs. **NPDH** strongly resists thermally induced racemization, whereas the enantiomers of **APDH** interconvert in solution at room temperature. Extensive intermolecular π-to-π interactions mediate the formation of single-handed supramolecular helixes of **APDH** from solution into the solid state. The gap separating the PDI subunits of **APDH** minimizes significantly the intramolecular π-to-π contact. Conversely, **NPDH** positions its PDI subunits within 3.2 Å of each other, resulting in collisions of their π-electron clouds. These collisions enhance the delocalization of electrons added to **NPDH**. Consequently, through-bond and through-space electronic delocalization have been married within a robust PDI-helicene framework. This combination of advantageous properties charts a clear course towards the application of **NPDH** and its derivatives in organic electronics. The delocalization of electrons along a persistent helical path anticipates the integration of this new molecular architecture into chiroptical and magnetic materials.

CCDC 1498856 (**APDH**) contains the crystallographic data for this paper. These data can be obtained free of charge from The Cambridge Crystallographic Data Centre.

Acknowledgements

We thank Dr. Brandon Fowler for assistance with HPLC, and Dr. Raúl Hernández Sánchez for thoughtful discussions. We thank the Nakanishi lab, particularly Dr. Ana Petrovic, Manuel Tamargo, and Dr. Nina Berova. We are deeply indebted to Ryan Hastie for the preparation of the ribbon graphics. N.S. is supported by the NSF Graduate Research Fellowship under grant number 11-44155. SCXRD was performed at the Shared Materials Characterization Laboratory at Columbia University. Use of the SMCL was made possible by funding from Columbia University. Primary support for this work was provided by the U.S. Department of Energy under award number DE-SC0014563.

Keywords: chirality · helicenes · mixed-valence compounds · perylene diimide · π–π interactions

How to cite: *Angew. Chem. Int. Ed.* **2016**, *55*, 13519–13523
Angew. Chem. **2016**, *128*, 13717–13721

[1] F. Würthner, C. R. Saha-Möller, B. Fimmel, S. Ogi, P. Leowanawat, D. Schmidt, *Chem. Rev.* **2016**, *116*, 962 – 1052.
[2] X. Zhan, A. Facchetti, S. Barlow, T. J. Marks, M. A. Ratner, M. R. Wasielewski, S. R. Marder, *Adv. Mater.* **2011**, *23*, 268 – 284.
[3] C. Huang, S. Barlow, S. R. Marder, *J. Org. Chem.* **2011**, *76*, 2386 – 2407.
[4] W. Jiang, Y. Li, Z. Wang, *Acc. Chem. Res.* **2014**, *47*, 3135 – 3147.
[5] F. Würthner, M. Stolte, *Chem. Commun.* **2011**, *47*, 5109 – 5115.
[6] Z. Liu, G. Zhang, Z. Cai, X. Chen, H. Luo, Y. Li, J. Wang, D. Zhang, *Adv. Mater.* **2014**, *26*, 6965 – 6977.
[7] D. Meng, D. Sun, C. Zhong, T. Liu, B. Fan, L. Huo, Y. Li, W. Jiang, H. Choi, T. Kim, et al., *J. Am. Chem. Soc.* **2016**, *138*, 375 – 380.
[8] Q. Wu, D. Zhao, A. M. Schneider, W. Chen, L. Yu, *J. Am. Chem. Soc.* **2016**, *138*, 7248 – 7251.
[9] Y. Zhong, B. Kumar, S. Oh, M. T. Trinh, Y. Wu, K. Elbert, P. Li, X. Zhu, S. Xiao, F. Ng, et al., *J. Am. Chem. Soc.* **2014**, *136*, 8122 – 8130.
[10] Y. Zhong, M. T. Trinh, R. Chen, W. Wang, P. P. Khlyabich, B. Kumar, Q. Xu, C.-Y. Nam, M. Y. Sfeir, C. Black, et al., *J. Am. Chem. Soc.* **2014**, *136*, 15215 – 15221.
[11] Y. Zhong, M. T. Trinh, R. Chen, G. E. Purdum, P. P. Khlyabich, M. Sezen, S. Oh, H. Zhu, B. Fowler, B. Zhang, et al., *Nat. Commun.* **2015**, *6*, 8242.
[12] M. Rickhaus, M. Mayor, M. Juríček, *Chem. Soc. Rev.* **2016**, *45*, 1542 – 1556.
[13] M. Gingras, *Chem. Soc. Rev.* **2013**, *42*, 968 – 1006.
[14] M. Gingras, G. Félix, R. Peresutti, *Chem. Soc. Rev.* **2013**, *42*, 1007 – 1050.
[15] M. Gingras, *Chem. Soc. Rev.* **2013**, *42*, 1051 – 1095.
[16] C. A. Liberko, L. L. Miller, T. J. Katz, L. Liu, *J. Am. Chem. Soc.* **1993**, *115*, 2478 – 2482.
[17] A. L. Sargent, J. Almolf, C. A. Liberko, *J. Phys. Chem.* **1994**, *98*, 6114 – 6117.
[18] C. Nuckolls, T. J. Katz, G. Katz, P. J. Collings, L. Castellanos, *J. Am. Chem. Soc.* **1999**, *121*, 79 – 88.
[19] T. Verbiest, S. Van Elshocht, M. Kauranen, L. Hellemans, J. Snauwaert, C. Nuckolls, T. J. Katz, A. Persoons, *Science* **1998**, *282*, 913 – 915.
[20] E. Anger, M. Srebro, N. Vanthuyne, L. Toupet, S. Rigaut, C. Roussel, J. Autschbach, J. Crassous, R. Réau, *J. Am. Chem. Soc.* **2012**, *134*, 15628 – 15631.
[21] M. Srebro, E. Anger, B. Moore II, N. Vanthuyne, C. Roussel, R. Réau, J. Autschbach, J. Crassous, *Chem. Eur. J.* **2015**, *21*, 17100 – 17115.
[22] C. Shen, G. Loas, M. Srebro-Hooper, N. Vanthuyne, L. Toupet, O. Cador, F. Paul, J. T. López Navarrete, F. J. Ramírez, B. Nieto-Ortega, et al., *Angew. Chem. Int. Ed.* **2016**, *55*, 8062 – 8066; *Angew. Chem.* **2016**, *128*, 8194 – 8198.
[23] P. Rajasingh, R. Cohen, E. Shirman, L. J. W. Shimon, B. Rybtchinski, *J. Org. Chem.* **2007**, *72*, 5973 – 5979.
[24] W. H. Laarhoven, T. H. J. H. M. Cuppen, R. J. F. Nivard, *Tetrahedron* **1970**, *26*, 4865 – 4881.
[25] Z. Yuan, Y. Xiao, X. Qian, *Chem. Commun.* **2010**, *46*, 2772 – 2774.
[26] Y. Li, L. Xu, T. Liu, Y. Yu, H. Liu, Y. Li, D. Zhu, *Org. Lett.* **2011**, *13*, 5692 – 5695.
[27] J. Vollbrecht, H. Bock, C. Wiebeler, S. Schumacher, H. Kitzerow, *Chem. Eur. J.* **2014**, *20*, 12026 – 12031.
[28] N. Miyaura, A. Suzuki, *Chem. Rev.* **1995**, *95*, 2457 – 2483.
[29] R. H. Martin, M.-J. Marchant, *Tetrahedron Lett.* **1972**, *13*, 3707 – 3708.
[30] T. Fujikawa, Y. Segawa, K. Itami, *J. Am. Chem. Soc.* **2015**, *137*, 7763 – 7768.
[31] J. Seibt, P. Marquetand, V. Engel, Z. Chen, V. Dehm, F. Würthner, *Chem. Phys.* **2006**, *328*, 354 – 362.
[32] J. Feng, Y. Zhang, C. Zhao, R. Li, W. Xu, X. Li, J. Jiang, *Chem. Eur. J.* **2008**, *14*, 7000 – 7010.
[33] K. A. Kistler, C. M. Pochas, H. Yamagata, S. Matsika, F. C. Spano, *J. Phys. Chem. B* **2012**, *116*, 77 – 86.
[34] F. Schlosser, M. Moos, C. Lambert, F. Würthner, *Adv. Mater.* **2013**, *25*, 410 – 414.
[35] K. M. Lefler, K. E. Brown, W. A. Salamant, S. M. Dyar, K. E. Knowles, M. R. Wasielewski, *J. Phys. Chem. A* **2013**, *117*, 10333 – 10345.
[36] E. A. Margulies, L. E. Shoer, S. W. Eaton, M. R. Wasielewski, *Phys. Chem. Chem. Phys.* **2014**, *16*, 23735 – 23742.
[37] A. P. de Silva, H. Q. N. Gunaratne, T. Gunnlaugsson, A. J. M. Huxley, C. P. McCoy, J. T. Rademacher, T. E. Rice, *Chem. Rev.* **1997**, *97*, 1515 – 1566.
[38] P. E. Hartnett, H. S. S. R. Matte, N. D. Eastham, N. E. Jackson, Y. Wu, L. X. Chen, M. A. Ratner, R. P. H. Chang, M. C. Hersam, M. R. Wasielewski, et al., *Chem. Sci.* **2016**, *7*, 3543 – 3555.
[39] S. K. Lee, Y. Zu, A. Herrmann, Y. Geerts, K. Müllen, A. J. Bard, *J. Am. Chem. Soc.* **1999**, *121*, 3513 – 3520.
[40] Y. Che, A. Datar, X. Yang, T. Naddo, J. Zhao, L. Zang, *J. Am. Chem. Soc.* **2007**, *129*, 6354 – 6355.
[41] T. M. Wilson, M. J. Tauber, M. R. Wasielewski, *J. Am. Chem. Soc.* **2009**, *131*, 8952 – 8957.
[42] T. M. Wilson, T. A. Zeidan, M. Hariharan, F. D. Lewis, M. R. Wasielewski, *Angew. Chem. Int. Ed.* **2010**, *49*, 2385 – 2388; *Angew. Chem.* **2010**, *122*, 2435 – 2438.
[43] Y. Wu, R. M. Young, M. Frasconi, S. T. Schneebeli, P. Spenst, D. M. Gardner, K. E. Brown, F. Würthner, J. F. Stoddart, M. R. Wasielewski, *J. Am. Chem. Soc.* **2015**, *137*, 13236 – 13239.

Received: August 12, 2016
Published online: September 26, 2016

